Hindawi
Advances in Civil Engineering
Volume 2019, Article ID 6717295, 13 pages
https://doi.org/10.1155/2019/6717295

Research Article

Experimental Investigation of the Permeability Measurement of Radial Flow through a Single Rough Fracture under Shearing Action

Ran Tan,[1] **Junrui Chai**,[2] **and Cheng Cao**[3]

[1]*Ph.D. Student, State Key Laboratory Base of Eco-hydraulic Engineering in Arid Area, Xi'an University of Technology, Xi'an 710048, China*
[2]*Professor, State Key Laboratory Base of Eco-hydraulic Engineering in Arid Area, Xi'an University of Technology, Xi'an 710048, China*
[3]*Master's Student, State Key Laboratory Base of Eco-hydraulic Engineering in Arid Area, Xi'an University of Technology, Xi'an 710048, China*

Correspondence should be addressed to Ran Tan; tr_xaut@163.com

Received 26 December 2018; Revised 27 March 2019; Accepted 3 April 2019; Published 2 May 2019

Academic Editor: Robert Černý

Water flow is commonly observed in rock fractures, and this flow has considerable significance in many aspects of rock engineering. In this study, seepage-stress coupled tests were performed on fractured rock masses using a computer-controlled direct shear device for rock with seepage control. The flow direction was radial. Eight types of test case were designed, and subgroup tests with varied normal stress, shear velocity, and roughness of fracture surface were conducted. The failure state of the fracture surface after the shear test, changes in shear stress, and fissure width and permeability under the above conditions were analyzed. The results include the following: the grain size of gouge fragments produced in rough fracture decreased with an increase in normal stress during shearing; the grain size of gouge fragments affected the fracture permeability; and the influence of shear velocity on the test results was mainly reflected after the peak strength. Additionally, a new expression describing fluid flow through fracture gouge is proposed.

1. Introduction

Joints with varying surface roughness and gouge content occur in underground rock masses and are the main channels of groundwater flow. These rock joints possess low shear strength [1]. When water seeps into rock joints, the rock is compressed and the joint surface is shear-dilated, closed, or even destroyed [2]. As a result, a complex seepage-stress state emerges. This complex stress state affects the stability of many large-scale rock engineering projects. Therefore, analysis of the hydraulic characteristics of fractured rock masses is an important topic in many areas of engineering, such as hydraulic structures, hydrogeology, rock mass mechanics, and mining engineering.

Few studies have considered the seepage-stress coupling effect of a joint fracture. The results reported to date have been obtained largely by laboratory test methods or experimental and numerical simulations. Researchers firstly considered the effect of normal stress on the joint surface, and many scholars carried out studies of normal stress and seepage, obtaining the classical cubic law. The mechanical behavior of rock is controlled mainly by shear displacement of discontinuities [3]. Shear dilation occurs during shear, but there are few studies on joint deformation characteristics under varying shear rate. Kleepmek et al. [4] believed that the peak shear strength of a rough fracture increases with displacement velocity. Li et al. [5] studied the strength characteristics of rock joints under different shear rates by using artificial concrete joint samples and found that the peak shear strength of rock joints decreased with the shear rate. However, the geometrical characteristics of the fracture surface also affect shear strength and hence weaken rock

asperities [6] and affect the relationship between the hydraulic aperture and mechanical aperture [7]. Fractures produce gouge material under shear deformation and normal stress. The gouge material fills in the fracture, affecting the overcurrent capability of the fracture. Chen et al. [8] believed that the plastic and liquefaction effects of fracture fillings significantly improve the permeability of fractures. And, Liu et al. [9] suggested that the modified cubic law cannot be used to simulate the motion of fracture fluid in the presence of gouge material.

In a partial laboratory test, through the modification of a biaxial or triaxial testing machine, a seepage device can be added to an original testing machine to create a device capable of testing the seepage-stress coupling system in joints [10–13]. The pore water pressure can be increased substantially in such a biaxial or triaxial testing machine, to be as high as 30–50 MPa [14, 15]. However, biaxial and triaxial tests do not consider the effect of direct shear; therefore, special test equipment must be developed to consider this effect.

Some researchers have completed the shear-seepage coupling tests under the condition of uniflow [15–18]. However, the geometric heterogeneity of a natural fracture surface leads to flow anisotropy, which is related to the direction of the injection pressure [19, 20]. Compared to uniflow flow, radial flow does not require consideration of the tightness issue on both sides of the joint sample; thus, many scholars have performed studies on radial flow. Tanikawa et al. [21] designed special test equipment that can use a thermocouple to heat nitrogen and calculate the seepage characteristics of granite fractures under thermo-hydro-mechanical conditions. Additionally, to study the effect of shearing stress, Yeo et al. [22] designed a special shear box for conducting shear-seepage tests under the condition of radial flow; however, its method of water injection was from the top down and the shear displacement was only 2 mm, to ensure sealing. A limitation of the tests was that the hydraulic pressure was low.

The above analysis of current experimental systems illustrates that a shear and radial flow coupling test technique for rock joints is still lacking. The test conditions do not tend to accurately represent natural conditions. In particular, there is no test that uses appropriate sealing technology. In addition, the maximum hydraulic pressure of the existing equipment is not high enough to reflect natural conditions. Based on the existing research and the urgent need to develop such equipment, we contacted the manufacturer to develop a new type of shear flow coupling test system. As a result, the YZS-600 microcomputer-controlled rock joint direct shear-seepage coupling test system was developed.

In this study, the newly designed system was used to test fluid flow in a series of cases in which normal stress, shear velocity, and roughness of fracture surface were varied.

2. Test System and Sample Preparation

2.1. Test System. The test system is composed of the main engine, servo oil source, stress system, multi-05 full-digital, multichannel, closed-loop control system, and sealed shear box. Figure 1 shows a photograph of the main components of the test system.

The shear loading frame is composed of a closed-loop controller, hydraulic servo oil source, force and displacement transducer, and sealed shear box. The shear force and normal force loading systems are controlled by an electrical displacement control (EDC) closed-loop controller developed by the Doli Company (Germany). The system has multiple measuring channels, and each channel can perform independent control, such as load control, deformation control, and displacement control. The testing machine can apply three boundary conditions, namely, constant normal displacement, constant normal load (CNL), and constant normal stiffness, in the normal direction. The stability of the normal rigidity can be ensured by feeding back the measured normal stress and normal deformation conditions during testing to the EDC. The EDC controller then adjusts the applied load as necessary to maintain constant rigidity. The hydraulic servo oil source controls the application of normal and shear loads. The force and displacement transducer monitors the normal and shear loads as well as the displacement change.

The samples are placed in a closed shear box, which is similar to a cube divided into upper and lower parts. The sample in the lower part of the shear box is fixed, whereas the sample in the upper part of the shear box is enveloped by an independent square rigid copper casting. The normal stress and shear stress act through pistons pushing on the rigid copper casting. The top of the shear box is arranged with a rigid roller to prevent the upper sample from moving independently. O-shaped rubber sealing rings are used where the sample is fixed to the shear box and around the normal and shear pistons to ensure that the shear box is airtight. A schematic of the shear box is shown in Figure 2.

The hydraulic loading system is composed of a water tank and nitrogen cylinder. Fixed pressure, with a maximum value of 3 MPa, is transmitted to the water tank through the relief valve on the nitrogen cylinder. Water is injected from the middle of the lower shear box base and then spreads onto the surface of the joint fissure. The water outlet is arranged on the surface of the lower shear box. This geometry allows for radial flow seepage mode. The mass of the water outflow is determined by an electronic scale and fed back to the computer. The flow direction is shown in Figure 3. The main technical parameters of the testing machine are provided by the manufacturer, as shown in Tables 1 and 2.

2.2. Sample Preparation. The shape of the sample box in this test system is a cylindrical flute; thus, the geometrical surface of the sample is a regular round shear surface. The fracture plane of natural rock is kaleidoscopic with gouge of different properties. Compared with natural rocks, the rock-like materials used in this study have better homogeneity and were selected for ease of specimen preparation [23, 24]. The rock-like samples were composed of a super strong gypsum sample with a regular sawtooth surface. To avoid inaccurate test results caused by differences in the physical and

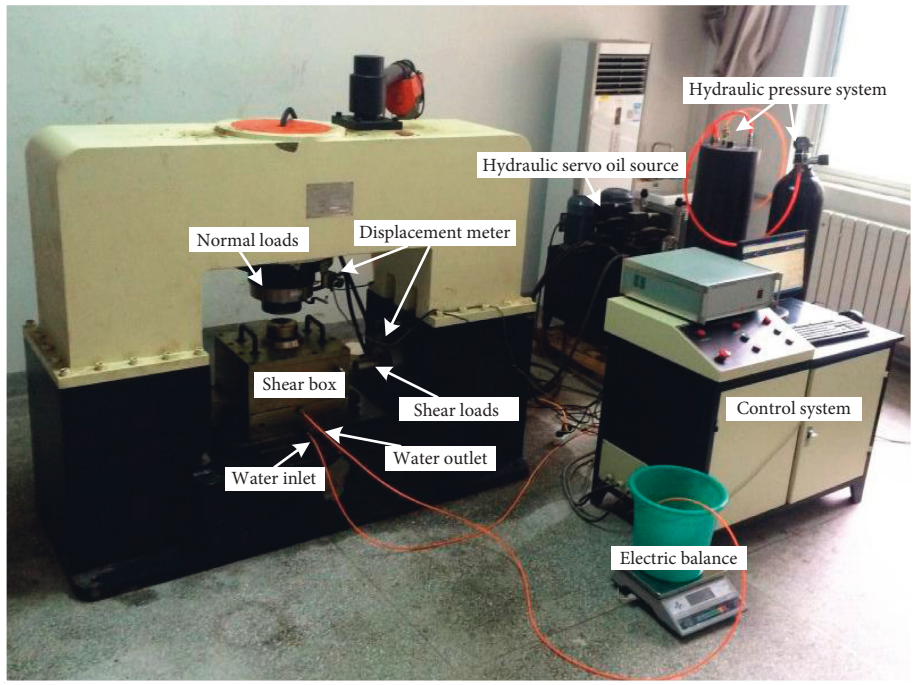

Figure 1: TJXW-600 microprocessor-control-coupled shear-seepage test system.

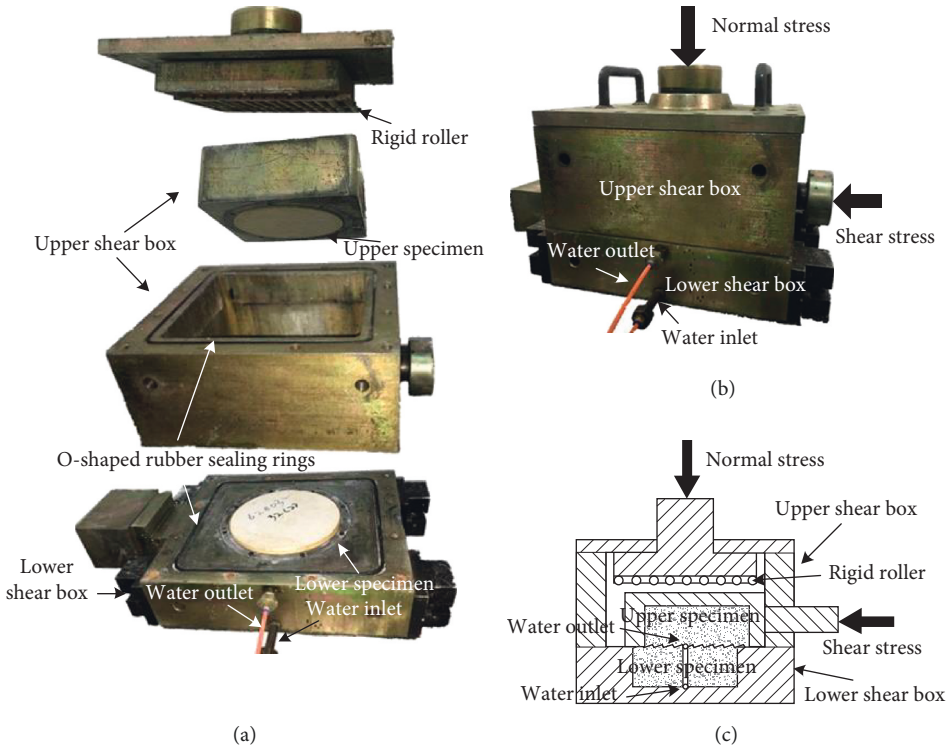

Figure 2: Schematic of the shear box structure.

mechanical properties and deformation intensity properties of the sample, the same test material was adopted for each batch of samples. The same mixing proportion and a mold of the same specifications were used to make each sample. The test material was extremely strong gypsum that is fully mixed with the proportions 25 g of water : 100 g of gypsum powder. The slurry, which has good liquidity, is similar to glue and was slowly cast in a rigid mould for coagulation over 10–15 min. The duration of the stripping operation was 40–60 min. The stripped sample is shown in Figure 4. Upon drying, the compressive strength of the samples reached 47.82 MPa, as shown in Table 3.

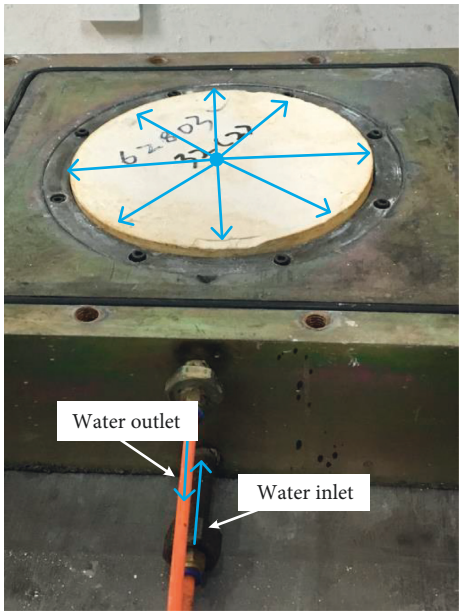

Figure 3: Flow direction of the seepage-stress coupling test system.

Table 1: Main technical parameters of the normal force and shear force electrohydraulic servo systems.

	Vertical force electrohydraulic servocontrol	Horizontal force electrohydraulic servocontrol
Maximal testing force	700 kN	
Effective measurement range of the testing force	20–80% F.S	
Indicating accuracy of the testing force	±1%	
Resolution of the testing force	1/200,000	
Displacement piston formation (force measured by a radial load sensor)	≥200 mm	≥100 mm
Measuring range of the displacement	0–200 mm	0–100 mm
Discrimination of the displacement	0.025 (5,000 yards)	
Indicating accuracy of the displacement	<±5% F.S	
Measuring range of the deformation	0–100 mm	
Indicating accuracy of the deformation	±5%	

Table 2: Main technical parameters of the hydraulic pressure stabilizing system.

Maximum pressure	3 MPa
Water storage	10 L
Measurement accuracy of the hydraulic pressure	
Stabilization accuracy of the hydraulic pressure	±0.1% of indication
Flow accuracy	

The rock-like samples were cylindrical with a basal diameter D of 200 mm and a height H of 75 mm. Two different types of fracture planes (smooth and rough) were considered as shown in Figure 4. The teeth on the plane of the rough sample were regularly spaced. The length of a single tooth was 10 mm, and there were 20 teeth (Figures 4(b) and 4(d)). The cross section of each tooth was a right triangle, and the undulant angle was 60° (Figure 4(b)). The smooth sample was free of undulant angles (Figures 4(a) and 4(c)).

Because of the differences in the joint surfaces of the samples and the existence of multiple sample directions for rough samples, many potential shear box placement orientations exist. Four feature combinations were selected in this test and are shown in Figure 5 (the pink arrow is the shear stress direction)—combination I: the upper and lower samples are smooth samples; combination II: the upper sample is a smooth sample, the lower sample is a rough sample, and the teeth ridges of the rough surface are oriented perpendicular to the shear direction; combination III: the upper and lower samples are rough samples, and the teeth ridges of both rough surfaces are oriented perpendicular to the shear direction; combination IV: the upper and lower samples of combination III are counter-rotated by 90°, so that the teeth ridges of both rough surfaces are oriented parallel to the shear direction.

2.3. Testing Procedure. Before the test, the gypsum sample was soaked until saturated. Subsequently, the following steps were performed:

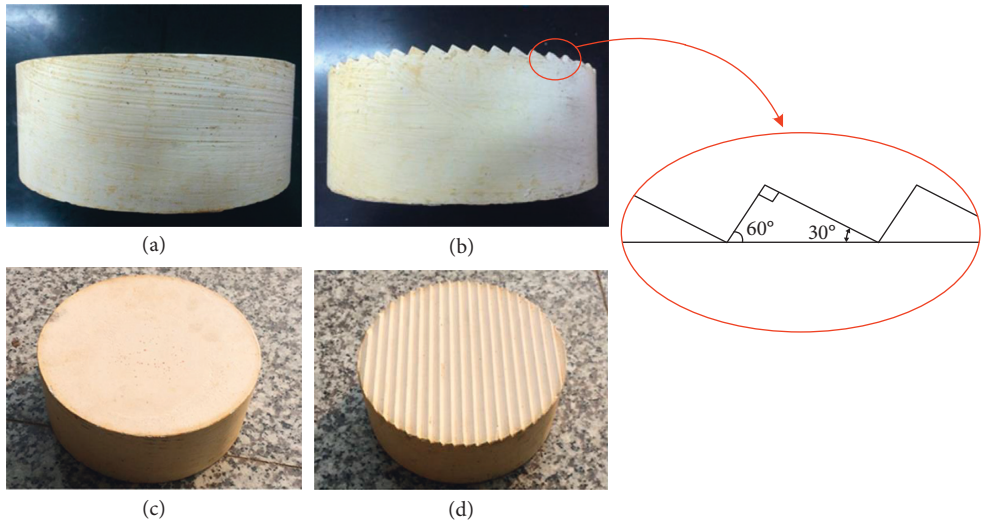

Figure 4: Structure of the test sample surface: (a) cross section of the smooth sample; (b) cross section of the rough sample; (c) surface of the smooth sample; (d) surface of the rough sample.

Table 3: Sample parameters.

Density (kg/m^3)	Poisson ratio	Elastic modulus (MPa)	Compressive strength (MPa)
1790	0.25	25700	47.82

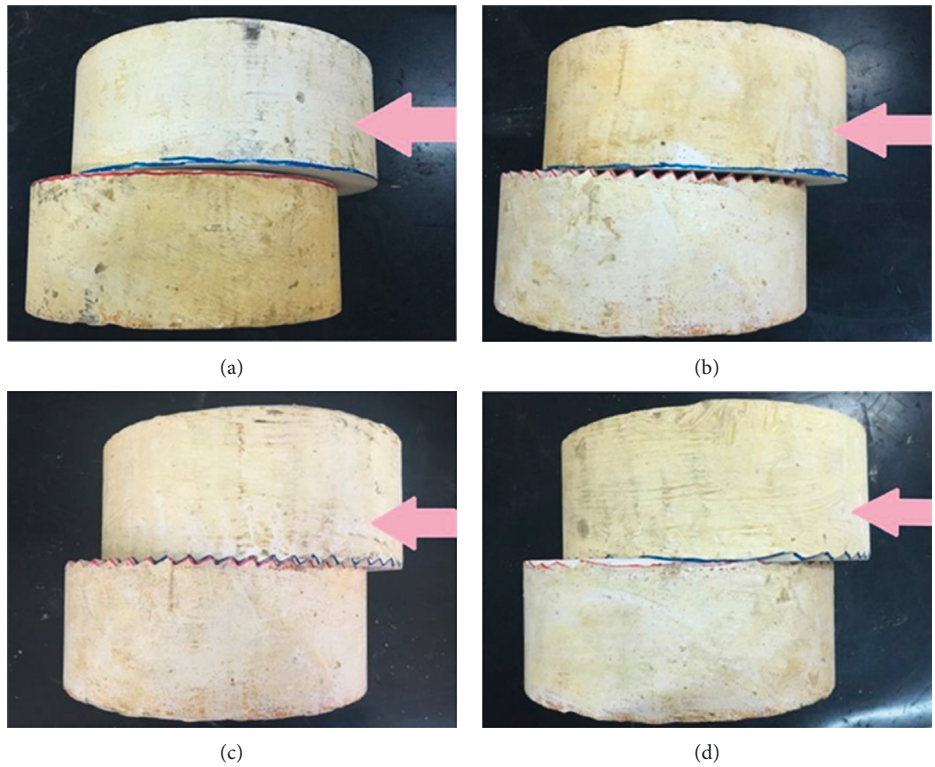

Figure 5: Rock-like sample combinations. (a) I. (b) II. (c) III. (d) IV.

Step 1. Open the instrument, place the rock-like sample in the shear box, and set the normal stress value and shear velocity in the computer program.

Step 2. Load the normal stress until it is stable.

Step 3. Open the nitrogen relief valve to increase the hydraulic pressure until the flow is stable.

Step 4. Begin shearing until the shearing displacement is maximized.

The boundary condition of this direct shear test was CNL, which is mainly used for rock slope stability analysis [25, 26]. Barton pointed out that when engineering problems related to a rock mass occur, the effective normal stress is commonly between 0.1 MPa and 2.0 MPa [27]. Therefore, the direct shear tests were carried out under a normal stress of about 2 MPa. Eight test cases were designed, as listed in Table 4.

The eight cases can be divided into three groups—A: (1) (2) (3), the normal stress increases with the other parameters remaining unchanged; B: (2) (4) (5), the shear velocity increases with the other parameters remaining unchanged; and C: (2) (6) (7) (8), the fissure surface combination mode is changed with the other parameters remaining unchanged.

3. Test Results and Discussion

3.1. Shear Stress Evolution. Three distinct stages of shear stress evolution with increasing shear displacement were observed, and these are compared in Figure 6. The shear stresses under all working conditions first increased rapidly, then decreased, before a final stable stage was reached. The value of shear stress after achieving stability was slightly higher than the initial value. The evolution of shear stress can be related to the extent of surface fracture damage.

3.2. Failure State of Fracture Surface. Experiments were performed to test whether the failure state of the fracture surface was directly related to the contact state of the rock-like samples.

For Group A, a larger normal stress led to higher shear stress (Figure 6(a)). Increasing shear stress increased damage to the sawtooth surface, as illustrated in Figure 7. After the shear test, abundant gouge material filled the fissures. These gouge material moved along the fissures due to fluid flow and shear displacement. It can be clearly seen that grain size of the gouge decreases with an increase in shear stress. Thus, the abrasive effect of shear stress on the fracture surface also increases. The shearing process can amplify the plastic and liquefaction effects of the gouge. Although all teeth were pulverized, the roots of the teeth were preserved and rough fissures remained which formed dominant channels for water flow, as shown in Figure 8.

For Group B, no obvious increase in peak shear strength was observed with an increase in shear velocity. After the shear tests, all teeth were pulverized and a large amount of gouge material filled the fissures (Figure 9). Residual shear strength increased with an increase in shear velocity (Figure 6(b)). After reaching the peak shear strength, under the action of gouge fragments and flow disturbance, increasing shear velocity caused the upper and lower sample blocks to slide along the fissures more easily, so the residual peak strength decreased with an increase in shear velocity. The size and distribution of gouge did not show obvious regularity.

For Group C, greater shear stress was required when the fracture surface was more complex (Figure 6(c)). The fracture surface failure varied across all four combinations. Figure 10(a) shows both upper and lower samples that are smooth. After the shear test, there were no obvious signs of damage, and the upper and lower surfaces remained smooth. It was not even possible to find traces of water pressure erosion. Figure 10(b) shows the case of the upper sample being smooth and the lower sample being rough. After loading normal stress, the smooth surface of the upper sample became textured due to contact with the lower sample. After loading shear stress, displacement lines were observed on the upper sample. A small portion of the lower sample was damaged due to the shear displacement. The sample surfaces shown in Figures 10(c) and 10(d) all began rough. The physical properties of the samples are the same, but the way they are placed in the shear box determines the final failure state. Case 2 (Figure 10(c)) is severely damaged, but Case 8 (Figure 10(d)) is hardly damaged. It can be seen that parameters such as undulant angle i, the Barton term for joint rock coefficient (JRC), and shear strength [28] are related to the shear direction and fracture surface matching of the samples.

3.3. Fissure Width. The distribution of fissure width b during shear can be expressed by the following equation [29]:

$$b = b_0 - \delta_n + \Delta\delta_n, \tag{1}$$

where b_0 is initial mechanical fissure width, δ_n is the change in mechanical fissure width due to normal stress, and $\Delta\delta_n$ is the change in mechanical aperture induced by shear deformation.

The fissures are filled with water before shearing, and the initial mechanical fissure width b_0 under the radial flow can be calculated by the following equation [22, 30]:

$$Q = \Delta H C b_0^3, \tag{2}$$

where Q is the steady state fluid flow rate, ΔH is the head difference, the constant $C = (2\pi/\ln(r_1/r_2))(g/12\mu)$ for radial flow, r_1 and r_2, represents the outside and inside radius of the fracture surface, respectively, g is the gravitational acceleration, and μ is the fluid dynamic viscosity.

Because the fracture widths are not always equal, the true initial fissure width b_0 in equation (2) is replaced by the equivalent hydraulic fissure width b_0', and equation (2) can be rewritten as follows:

$$b_0' = \left(\frac{12\mu Q}{\Delta H C' g}\right)^{1/3}, \tag{3}$$

where $C' = 2\pi/\ln(r_1/r_2)$.

Under the CNL boundary condition, δ_n is equal to 0. Finally, the equivalent fissure width can be obtained from the following equation:

$$b' = b_n' + \Delta\delta_n. \tag{4}$$

The calculated data points are grouped in Figure 11.

In Figure 11, when the test begins, there is only normal stress and hydraulic pressure, and the fissure width is

Table 4: Experimental cases.

Case	Normal stress (MPa)	Shear velocity (mm/s)	Hydraulic pressure (MPa)	Type of sample combination
1	1.27	0.25	0.6	III
2	1.91	0.25		III
3	2.23	0.25		III
4	1.91	0.33		III
5	1.91	0.42		III
6	1.91	0.25		I
7	1.91	0.25		II
8	1.91	0.25		IV

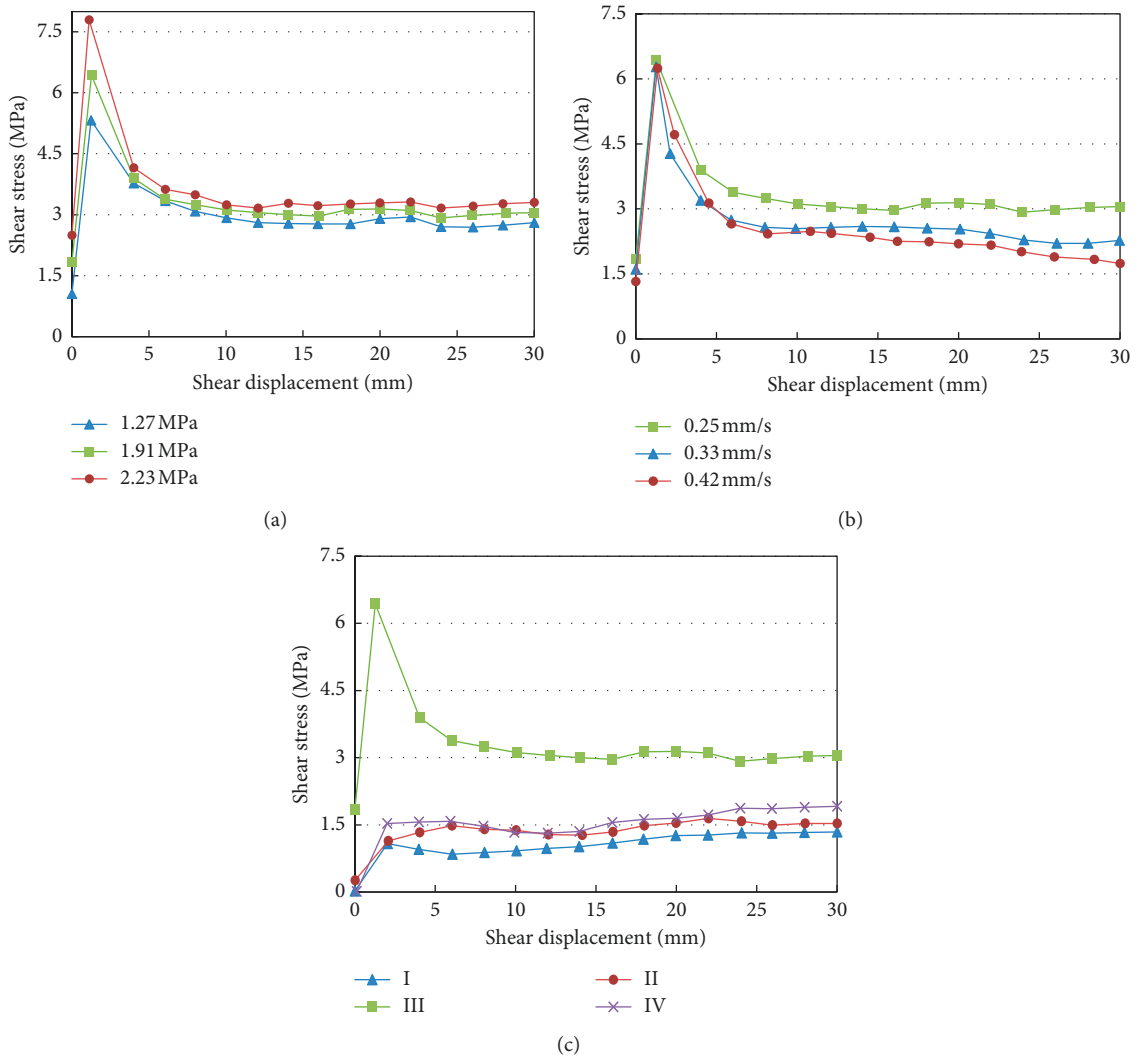

Figure 6: Evolution of shear stress with increasing shear displacement. (a) Increasing normal stress. (b) Increasing shear velocity. (c) Changes in the fissure plane combination mode.

relatively small. After the shear stress is loaded, the fracture surface is dislocated and the teeth are gradually destroyed. With increasing shear displacement, the fracture surface is gradually destroyed and the fissure width gradually increases. The following conclusions can be obtained according to the figures for each group:

Group A: there is more compaction of the upper and lower samples when the normal stress is larger. After the shear stress is loaded, the teeth of the fracture surface are destroyed, gouge in the fracture is pressed tightly, and the fissure width exhibits a decreasing trend.

(a) (b) (c)

Figure 7: Group A fracture surfaces after the shear tests. (a) Case 1. (b) Case 2. (c) Case 3.

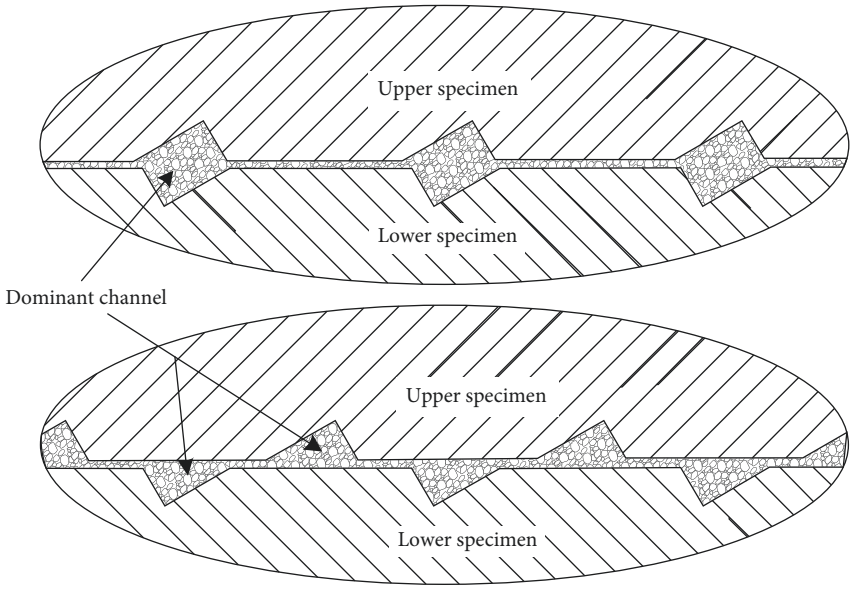

Figure 8: Dominant channels for water flow after the shear test.

Group B: as shown in Figures 6(b) and 9, under the action of gouge and flow disturbance, an increase in shear velocity makes the upper and lower surfaces slide more easily. The fissure width decreases with an increase in the shearing velocity of the fracture surface.

Group C: Figure 10 shows that after the shear test, except for combination III, evolution of the fracture surface of the other three groups is relatively complete. The fissure width of combination III increases dramatically during shear, and the final value is much higher than for the other three cases (Figure 11(c)). The other three cases remain stable. This suggests that the gouge material has a strong influence on fissure width.

(a) (b) (c)

Figure 9: Group B fracture surfaces after the shear tests. (a) Case 2. (b) Case 4. (c) Case 5.

(a) (b) (c) (d)

Figure 10: Group C fracture surfaces after the shear tests. (a) Case 6. (b) Case 7. (c) Case 2. (d) Case 8.

3.4. Hydraulic Conductivity. In Figure 12, the flow increases with shear displacement after the rough fracture surfaces are damaged. The flow of the undisturbed (i.e., smooth) fracture surfaces remains stable. It can be seen that the permeability of rough fractures increase with shear displacement.

Hydraulic conductivity can be expressed as

$$k = \frac{K\rho g}{\mu}, \tag{5}$$

where K is permeability and ρ is liquid density.

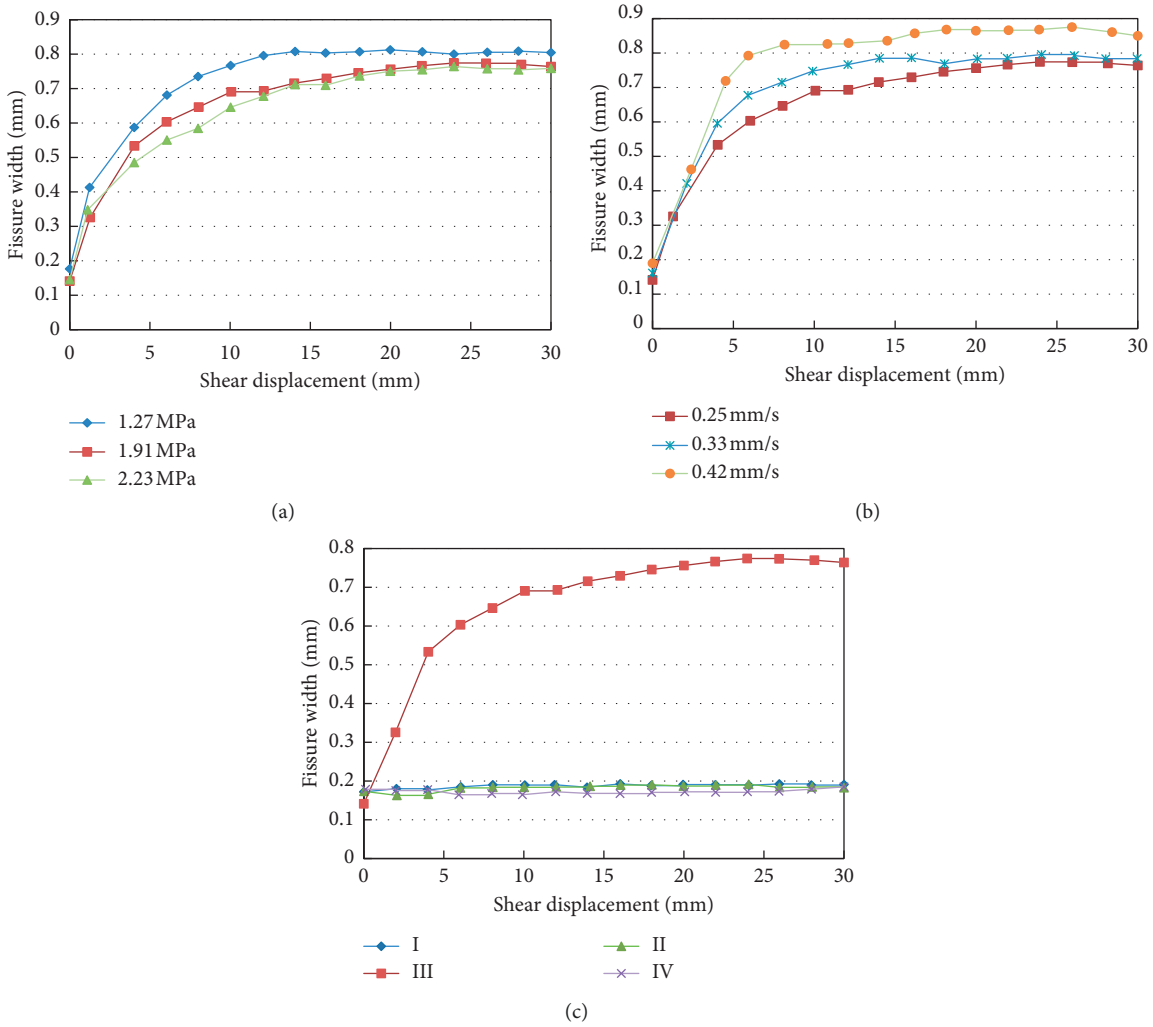

Figure 11: Evolution in fissure width with increasing shear displacement. (a) Increasing normal stress. (b) Increasing shear velocity. (c) Changes in the fissure plane combination mode.

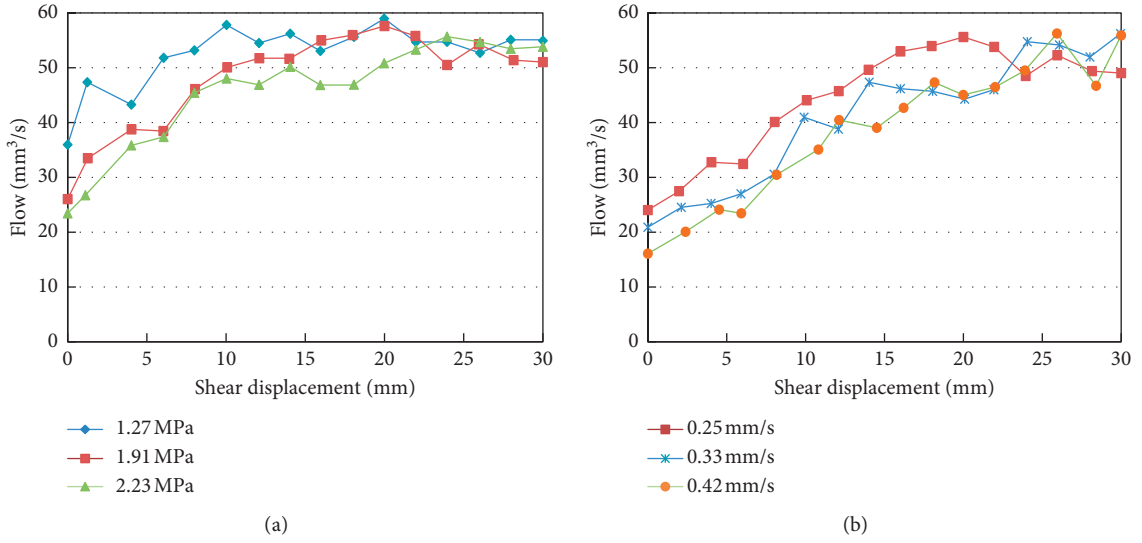

Figure 12: Continued.

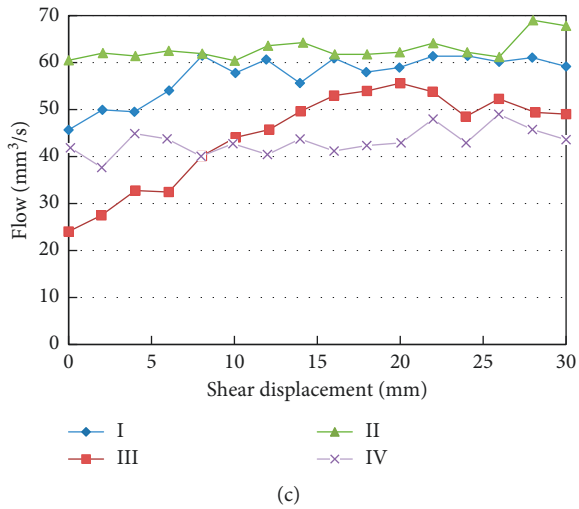

Figure 12: Variations in flow with increasing shear displacement. (a) Increasing normal stress. (b) Increasing shear velocity. (c) Changes in the fissure plane combination mode.

After the teeth of the rough fracture surfaces are pulverized, abundant gouge material is produced in the fissures. The gouge fills the dominant channels of water flow and the fracture. The gouge is a porous media. As can be seen from Figure 8, normal stress changes the grain size of the gouge fragments. Liu et al. obtained the following equation by experiment [9]:

$$K = \frac{mb}{D_m} + n, \tag{6}$$

where b is fissure width, D_m is grain size, and m and n are coefficients related to the geometric parameters of both fracture and rock. Equation (6) implies that K increases with increasing b/D_m.

Considering the obvious change in permeability with shear displacement and the larger change in gouge grain size under different normal stress N, equivalent fissure width b' and shear displacement d can be shown to follow a natural logarithmic relationship (Figure 13), written as follows:

$$b' = \alpha \ln(d) + \beta, \tag{7}$$

where α, β are parameters, $d > 0$.

Figure 14 and Table 5 show that α and β are linear with normal stress N, written as follows:

$$\begin{aligned} \alpha &= aN + b, \\ \beta &= cN + d. \end{aligned} \tag{8}$$

Hydraulic conductivity under different normal stress can be obtained by substituting equations (6) and (7) into equation (5):

$$k = \frac{\left(m\left((\alpha \ln(d) + \beta)/D_m\right) + n\right)\rho g}{\mu}. \tag{9}$$

In addition, for this study the values of a, b, c, and d in equation (8) are 0.251, 0.1001, −0.1522, and 0.6036, respectively, when equation (9) is applied to other researches; the values of α and β can be ensured by referring equations (7) and (8) and the test conditions.

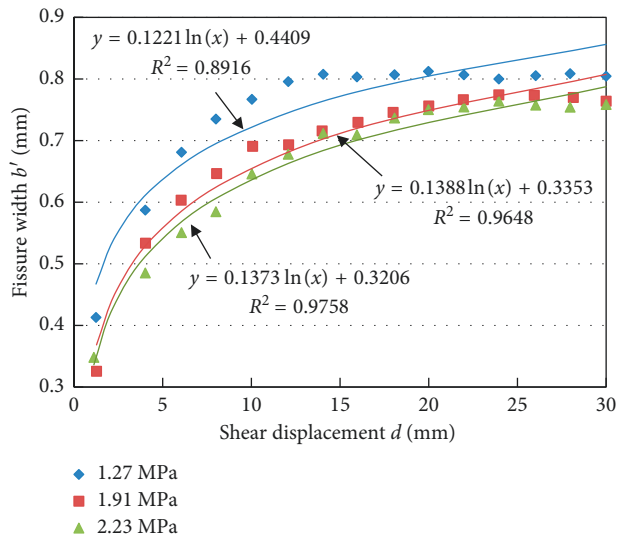

Figure 13: Change in fissure width b' with increasing shear displacement d.

4. Conclusions

This study examined the hydromechanical coupling of a single rough fracture. The microcomputer-controlled rock joint direct shear-seepage coupling test system used in this study was based on advanced virtual technology. Under radial flow, eight test cases of artificial fractures were tested to observe changes in deformation behavior with changing normal stress, shear velocity, and roughness of the fracture surface. After testing, variations in the mechanical properties and the permeability of rough fracture surfaces during shear were determined.

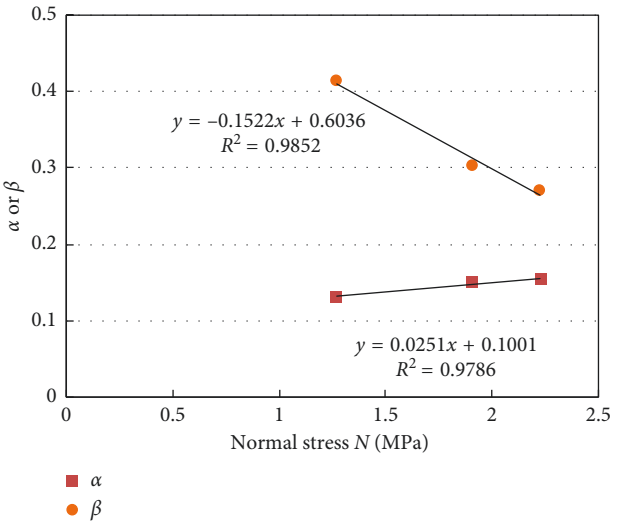

Figure 14: Change of α, β with normal stress N.

Table 5: α and β for different normal stresses.

Normal stress N (MPa)	α	β	R^2
1.27	0.1313	0.4137	0.8456
1.91	0.1501	0.3025	0.9275
2.23	0.1547	0.271	0.9713

The grain size of gouge produced by rough fracture surface deterioration was shown to decrease with an increase in normal stress during shear. The fissure width of rough fractures was determined mainly by gouge fragment size. High normal stress was shown to cause liquefaction or plasticization of gouge material. Gouge filled the preserved roots of teeth on rough surfaces to form the dominant channels of water flow. The grain size of the gouge affected fracture permeability. The influence of shear velocity on the test results was mainly observed after the peak strength; the faster the shear velocity, the smaller the observed shear stress. A shared orientation of shear direction and teeth on the fracture surface had a considerable influence on the shear stress, undulant angle, and JRC. The fissure width of rough fractures was shown to correlate with the change in shear displacement. Therefore, a new expression describing fluid flow in gouge-filled fractures under different normal stress was proposed. In this study, the parameters α and β of equation (7) were related to normal stress, and α increased, while β decreased, with increasing normal stress. When equation (7) was used in other tests, the reference values of α and β were confirmed by equation (8). Because of the limitations of sample processing and testing equipment, only three normal stress tests were carried out in this study. However, although our data were somewhat limited, this expression should provide a reference for the study of permeability of rock joints.

As water flows from the center of the specimen to the edge, there is a head drop and a gradient in hydrostatic pressure forms across the specimen (from the applied pressure on the inside to zero on the outside). Future works will focus on the influence of this gradient on the overall effective stress.

Data Availability

The experimental data used to support the findings of this study are included within the article.

Conflicts of Interest

The authors declare that there are no conflicts of interest regarding the publication of this paper.

Acknowledgments

This study was supported by the National Natural Science Foundation of China (51679197) and Program 2013KCT-15 for the Shaanxi Provincial Key Innovative Research Team.

References

[1] N. Barton, "The shear strength of rock and rock joints," *International Journal of Rock Mechanics and Mining Sciences & Geomechanics Abstracts*, vol. 13, no. 9, pp. 255–279, 1976.

[2] B. Li, Z. Zhao, Y. Jiang, and L. Jing, "Contact mechanism of a rock fracture subjected to normal loading and its impact on fast closure behavior during initial stage of fluid flow experiment," *International Journal for Numerical and Analytical Methods in Geomechanics*, vol. 39, no. 13, pp. 1431–1449, 2015.

[3] M. Bahaaddini, G. Sharrock, and B. K. Hebblewhite, "Numerical direct shear tests to model the shear behaviour of rock joints," *Computers and Geotechnics*, vol. 51, pp. 101–115, 2013.

[4] M. Kleepmek, S. Khamrat, T. Thongprapha, and K. Fuenkajorn, "Displacement velocity effects on rock fracture shear strengths," *Journal of Structural Geology*, vol. 90, pp. 48–60, 2016.

[5] H. Li, B. Liu, H. Feng, and L. Zhang, "Study of deformability behaviour and failure mechanism by simulating rock joints sample under different loading conditions," *Rock and Soil Mechanics*, vol. 29, no. 7, pp. 1741–1752, 2008.

[6] F. Johansson and H. Stille, "A conceptual model for the peak shear strength of fresh and unweathered rock joints," *International Journal of Rock Mechanics and Mining Sciences*, vol. 69, pp. 31–38, 2014.

[7] X. Xiong, B. Li, Y. Jiang, T. Koyama, and C. Zhang, "Experimental and numerical study of the geometrical and hydraulic characteristics of a single rock fracture during shear," *International Journal of Rock Mechanics and Mining Sciences*, vol. 48, no. 8, pp. 1292–1302, 2011.

[8] J.-G. Chen, J.-L. Yang, and J.-F. Zhang, "Effect of expansive fillings on fracture seepage," *Mining Science and Technology (China)*, vol. 19, no. 6, pp. 824–828, 2009.

[9] R. Liu, H. Jing, L. He, T. Zhu, L. Yu, and H. Su, "An experimental study of the effect of fillings on hydraulic properties of single fractures," *Environmental Earth Sciences*, vol. 76, p. 684, 2017.

[10] A. Makurat, N. Barton, N. Rad, and S. Bandis, "Joint conductivity variation due to normal and shear deformation," *International Journal of Rock Mechanics and Mining Sciences & Geomechanics Abstracts*, vol. 28, no. 2-3, p. A150, 1991.

[11] C. Collettini, G. Di Stefano, B. Carpenter et al., "A novel and versatile apparatus for brittle rock deformation,"

International Journal of Rock Mechanics and Mining Sciences, vol. 66, pp. 114–123, 2014.

[12] G. Yin, C. Jiang, J. G. Wang, and J. Xu, "Combined effect of stress, pore pressure and temperature on methane permeability in anthracite coal: an experimental study," *Transport in Porous Media*, vol. 100, no. 1, pp. 1–16, 2013.

[13] A. P. Niemi, T. A. Vaittinen, J. A. Vuopio, and J. P. Pöllä, "Simulation of heterogeneous flow in a natural fracture under varying normal stress," *International Journal of Rock Mechanics and Mining Sciences*, vol. 34, no. 3-4, pp. 227.e1–227.e11, 1997.

[14] D. Ma, X. X. Miao, Z. Q. Chen, and X. B. Mao, "Experimental investigation of seepage properties of fractured rocks under different confining pressures," *Rock Mechanics and Rock Engineering*, vol. 46, no. 5, pp. 1135–1144, 2013.

[15] D. Ma, X. X. Miao, G. H. Jiang, H. B. Bai, and Z. Q. Chen, "An experimental investigation of permeability measurement of water flow in crushed rocks," *Transport in Porous Media*, vol. 105, no. 3, pp. 571–595, 2014.

[16] Y. Ohnishi and P. Dharmaratne, "Shear behaviour of physical models of rock joints under constant normal stiffness conditions," in *Proceedings of the International Symposium Rock Joints*, pp. 267–273, Loen, Norway, June 1990.

[17] N. Xie, J. Yang, and J. Shao, "Study on the hydromechanical behavior of single fracture under normal stresses," *KSCE Journal of Civil Engineering*, vol. 18, no. 6, pp. 1641–1649, 2014.

[18] G. Wang, Y. Jiang, W. Wang, and T. Li, "Development and application of an improved numeric control shear-fluid coupled apparatus for rock joint," *Rock and Soil Mechanics*, vol. 33, pp. 3456–3465, 2014.

[19] Y. Méheust and J. Schmittbuhl, "Flow enhancement of a rough fracture," *Geophysical Research Letters*, vol. 27, no. 18, pp. 2989–2992, 2000.

[20] Y. Méheust and J. Schmittbuhl, "Geometrical heterogeneities and permeability anisotropy of rough fracture," *Journal of Geophysical Research: Solid Earth*, vol. 106, no. B2, pp. 2089–2102, 2001.

[21] W. Tanikawa, O. Tadai, and H. Mukoyoshi, "Permeability changes in simulated granite faults during and after frictional sliding," *Geofluids*, vol. 14, no. 4, pp. 481–494, 2014.

[22] I. W. Yeo, M. H. de Freitas, and R. W. Zimmerman, "Effect of shear displacement on the aperture and permeability of a rock fracture," *International Journal of Rock Mechanics and Mining Sciences*, vol. 35, no. 8, pp. 1051–1070, 1998.

[23] H. Cheng, X. Zhou, J. Zhu, and Q. Qian, "The effects of crack openings on crack initiation, propagation and coalescence behavior in rock-like materials under uniaxial compression," *Rock Mechanics and Rock Engineering*, vol. 49, no. 9, pp. 3481–3494, 2016.

[24] C. Cao, Z. Xu, J. Chai, Y. Qin, and R. Tan, "Mechanical and hydraulic behaviors in a single fracture with asperities crushed during shear," *International Journal of Geomechanics*, vol. 18, no. 11, article 04018148, 2018.

[25] N. Barton and K. Bakhtar, *Rock Joint Description and Modelling for the Hydro-Thermo-Mechanical Design of Nuclear Waste Repositories*, Mining Research Laboratory, Ottawa, ON, Canada, 1983.

[26] A. K. Shrivastava and K. S. Rao, "Shear behaviour of rock joints under CNL and CNS boundary conditions," *Geotechnical and Geological Engineering*, vol. 33, no. 5, pp. 1205–1220, 2015.

[27] N. Barton, "Review of a new shear-strength criterion for rock joints," *Engineering Geology*, vol. 7, no. 4, pp. 287–332, 1973.

[28] Z. C. Tang, Y. Y. Jiao, L. N. Y. Wong, and X. C. Wang, "Choosing appropriate parameters for developing empirical shear strength criterion of rock joint: review and new insights," *Rock Mechanics and Rock Engineering*, vol. 49, no. 11, pp. 4479–4490, 2016.

[29] T. Esaki, S. Du, Y. Mitani, K. Ikusada, and L. Jing, "Development of a shear-flow test apparatus and determination of coupled properties for a single rock joint," *International Journal of Rock Mechanics and Mining Sciences*, vol. 36, no. 5, pp. 641–650, 1999.

[30] M. Gutierrez, L. E. Øino, and R. Nygård, "Stress-dependent permeability of a de-mineralised fracture in shale," *Marine and Petroleum Geology*, vol. 17, no. 8, pp. 895–907, 2000.